*Protein Science* (2000), *9*:867–877. Cambridge University Press. Printed in the USA.


# Conformational transitions and fibrillation mechanism of human calcitonin as studied by high-resolution solid-state $^{13}C$ NMR

MIYA KAMIHIRA,[1] AKIRA NAITO,[1] SATORU TUZI,[1] ATSUKO Y. NOSAKA,[2] AND HAZIME SAITÔ[1]

[1]Department of Life Science, Himeji Institute of Technology, Harime Science Garden City, Kamigori, Hyogo 678-1297, Japan
[2]International Research Laboratories, Ciba-Geigy Japan Ltd., PO Box 1, Takarazuka 665, Japan

(RECEIVED November 10, 1999; FINAL REVISION February 24, 2000; ACCEPTED March 10, 2000)

**Abstract**

Conformational transitions of human calcitonin (hCT) during fibril formation in the acidic and neutral conditions were investigated by high-resolution solid-state $^{13}C$ NMR spectroscopy. In aqueous acetic acid solution (pH 3.3), a local $\alpha$-helical form is present around Gly10, whereas a random coil form is dominant as viewed from Phe22, Ala26, and Ala31 in the monomer form on the basis of the $^{13}C$ chemical shifts. On the other hand, a local $\beta$-sheet form as viewed from Gly10 and Phe22, and both $\beta$-sheet and random coil as viewed from Ala26 and Ala31 were detected in the fibril at pH 3.3. The results indicate that conformational transitions from $\alpha$-helix to $\beta$-sheet, and from random coil to $\beta$-sheet forms occurred in the central and C-terminus regions, respectively, during the fibril formation. The increased $^{13}C$ resonance intensities of fibrils after a certain delay time suggests that the fibrillation can be explained by a two-step reaction mechanism in which the first step is a homogeneous association to form a nucleus, and the second step is an autocatalytic heterogeneous fibrillation. In contrast to the fibril at pH 3.3, the fibril at pH 7.5 formed a local $\beta$-sheet conformation at the central region and exhibited a random coil at the C-terminus region. Not only a hydrophobic interaction among the amphiphilic $\alpha$-helices, but also an electrostatic interaction between charged side chains can play an important role for the fibril formation at pH 7.5 and 3.3 acting as electrostatically favorable and unfavorable interactions, respectively. These results suggest that hCT fibrils are formed by stacking antiparallel $\beta$-sheets at pH 7.5 and a mixture of antiparallel and parallel $\beta$-sheets at pH 3.3.

**Keywords:** autocatalytic reaction; conformational transition; fibril formation; human calcitonin; solid-state $^{13}C$ NMR

Calcitonin (CT) is a peptide hormone consisting of 32 amino acid residues that contains an intrachain disulfide bridge between Cys1 and Cys7 and a proline amide at the C-terminus. In mammals, CT plays a central role in calcium–phosphorus metabolism as a thyroid hormone (Copp et al., 1962; Kumar et al., 1963; Austin & Heath, 1981), and the entire molecule is necessary for full biological activity (Copp, 1970). Thus, CT has been treated as a useful drug for various bone disorders such as Paget's disease and osteoporosis. However, human calcitonin (hCT) has a tendency to associate to form fibril precipitate in aqueous solution. Such amyloid fibril formations are well known as a cause of amyloid deposits in Alzheimer's disease (Sipe, 1992). In addition, prion diseases such as sheep scrapie and bovine spongiform encephalopathy (BSE) have been reported to be related to disorders of the protein conformation in which one folds normally and another aggregates into the amyloid fibril (Cohen et al., 1994; Taubes, 1996). It is therefore very important to clarify the fibrillation process and molecular mechanism not only to contribute to the further improvement of hCT with the long-term stability (Arvinte & Ryman, 1992), but also to gain insight into the mechanism of amyloid formation in general, which causes many kinds of such diseases.

Conformations of hCT in several solvents have been studied by solution NMR spectroscopy. In TFE/$H_2O$, hCT forms a helical structure between the residues 9 and 21 (Doi et al., 1990). A short double-stranded antiparallel $\beta$-sheet form, however, was observed

Reprint requests to: Hazime Saitô, Department of Life Science, Himeji Institute of Technology, 3-2-1 Kouto, Kamigori, Hyogo 678-1297, Japan; e-mail: saito@sci.himeji-tech.ac.jp.

*Abbreviations:* ATR-FTIR, attenuated total reflection Fourier transform infrared; CD, circular dichroism; CP-MAS, cross-polarization magic-angle spinning; CT, calcitonin; DD-MAS, dipolar decoupled magic-angle spinning; DMSO, dimethyl sulfoxide; Fmoc, 9-fluorenylmethoxycarbonyl; Fmoc-Osu, 9-fluorenylmethyl N-succinimidyl carbonate; FTIR, Fourier transform infrared spectroscopy; hCT, human calcitonin; hCT-SH, reduced form of human calcitonin; HPLC, high-performance liquid chromatography; NOESY, nuclear Overhauser enhancement spectroscopy; sCT, salmon calcitonin; TFE, 2,2,2-trifluoroethanol; TFA, trifluoroacetic acid; T-FTIR, transmission Fourier transform infrared; TMS, tetramethylsilane; TOSS, total suppression of spinning side bands.

in the central region made by residues 16–21 in DMSO/$H_2O$ (Motta et al., 1991b). It was suggested that hCT exhibits an amphiphilic nature when it forms an $\alpha$-helix (Epand et al., 1983). However, the secondary structure of hCT in $^2H_2O$ was shown to take totally random coil as determined from the $^1H$ chemical shift data (Wüthrich, 1976). Subsequent studies by two-dimensional (2D) NOESY and CD measurements indicated that it adopts an extended conformation with high flexibility in aqueous solution (Kern et al., 1993). Recently, $\alpha$-helical conformation is reported to be present in the central region of hCT in aqueous *acidic* solution, although it is shorter than that in TFE/$H_2O$ (Jeon et al., 1998). Similarly, NMR studies showed that salmon calcitonin (sCT) also forms an amphiphilic $\alpha$-helical structure in the central region in TFE/$H_2O$ (Meyer et al., 1991), methanol/$H_2O$ (Meadows et al., 1991), and SDS micelle (Motta et al., 1991a). It has been reported that sCT has a high activity and stability as a drug (Habener et al., 1971; Rittel et al., 1976) and the fibrillation process is much slower than in hCT (Arvinte et al., 1993).

Electron microscopic studies of hCT fibrils have revealed that they consist of fibers of 8 nm in diameter, which often associate with one another (Sieber et al., 1970). Turbidity measurements of the kinetics of hCT fibrillation have demonstrated that the fibrillation process can be explained by a double nucleation mechanism (Ferrone et al., 1980, 1985; Samuel et al., 1990; Arvinte et al., 1993). They proposed that fibrillation starts with an homogeneous nucleation step from hCT monomers, and afterward fibrillation continues with development of new fibrils from existing ones, which is referred to as the heterogeneous nucleation step. It has been also shown by CD, fluorescence, and FTIR (Arvinte et al., 1993) that hCT fibrils have $\alpha$-helical and $\beta$-sheet components. Transmission (T-FTIR) and attenuated total reflection FTIR (ATR-FTIR) experiments have indicated that hCT initially adopts a random coil conformation, and subsequently, fractions of the $\alpha$-helical and intermolecular parallel $\beta$-sheet forms simultaneously increased (Bauer et al., 1994). Two-dimensional NMR measurements of the time course of the fibrillation process have shown that the peaks from residues in the N-terminal (Cys1–Cys7) and the central (Met8–Pro23) regions are broadened and disappear earlier than those in the C-terminal region (Gln24–Pro32) (Kanaori & Nosaka, 1995). These findings indicate that the $\alpha$-helices are bundled together in the first homogeneous nucleation process. Subsequently, it appears that larger fibrils grow as the second heterogeneous process (Arvinte et al., 1993). However, local structures and characteristics of hCT in the fibril have not been obtained directly by solution NMR spectroscopy, because the intrinsically broadened signals from the fibril components cannot be observed.

In the present study, we aimed to clarify the secondary structure and fibrillation kinetics of site specifically $^{13}C$-labeled hCT (Scheme 1) by high resolution solid-state $^{13}C$ NMR spectroscopy, which is a more suitable means for the fibril state in addition to the solution state. High-resolution solid-state $^{13}C$ NMR spectroscopy has proved to be a powerful tool for studying the secondary structure of polypeptides based on the conformation-dependent $^{13}C$ chemical shift values (Saitô, 1986; Saitô & Ando, 1989; Saitô et al., 1998). The use of the $^{13}C$ chemical shifts to evaluate the secondary structure of protein has been extended to the liquid-state $^{13}C$ NMR spectroscopy (Wishart et al., 1991; Wishart & Sykes, 1994). Site specifically $^{13}C$-labeled carbonyl groups for Gly10 and Phe22 or methyl carbons at Ala26 and Ala31 in hCT provided a clue to the local conformations and dynamics in the vicinity of the specific sites. Particularly, these labeled sites were chosen to give the structure information of both central and C-terminal regions. It is emphasized that measurements of two types of high-resolution solid-state NMR spectroscopy, DD-MAS (one pulse excitation with dipolar decoupled-magic angle spinning) and CP-MAS (cross-polarization magic-angle spinning) made it possible to study the respective conformations of the solution and fibril states, simultaneously, in the same sample. Further, we analyzed fibrillation kinetics based on both NMR and CD measurements to characterize the molecular mechanism of fibril formation.

1 5 10 15
Cys-Gly-Asn-Leu-Ser-Thr-Cys-Met-Leu-Gly-Thr-Tyr-Thr-Gln-Asp-
20 25 30
Phe-Asn-Lys-Phe-His-Thr-Phe-Pro-Gln-Thr-Ala-Ile-Gly-Val-Gly-
Ala-Pro-$NH_2$

**Scheme 1.** Amino acid sequence of hCT.

## Results

### *Characterization of the hCT fibrils by visual and electron microscope observations*

In this paper, we have mainly used two types of selectively $^{13}C$-labeled hCTs synthesized at Himeji Institute of Technology: (I) [1-$^{13}C$]Phe22, [3-$^{13}C$]Ala31-labeled hCT, and (II) [1-$^{13}C$]Gly10, [3-$^{13}C$] Ala26-labeled hCT. When II was dissolved in 0.015 M acetic acid solution (pH 3.3), viscosity of the solution increased to develop into a turbid gel during the first 3 h, and afterward the turbidity was slightly increased. On the other hand, when II was dissolved in 0.1 M sodium acetate solution (pH 7.5), which is much lower concentration (1.5 mg/mL) compared to that in the acidic solution, turbidity was already seen after 2 h of dissolution, but did not develop into a gel state. Figure 1 shows the electron micrographs from the suspension of II after incubating 2 or 3 days at pH 3.3 (Fig. 1A) and 7.5 (Fig. 1B), respectively. Long fibrils with the diameter of 7–8 nm were observed in the suspension of II at pH 3.3 (Fig. 1A), whereas the aggregation of short fibrils with the diameter of 6–10 nm appeared at pH 7.5 (Fig. 1B).

### *$^{13}C$ NMR spectra of site specifically $^{13}C$-labeled hCT*

Figure 2 shows the $^{13}C$ DD- and CP-MAS NMR spectra of site specifically $^{13}C$-labeled hCT, [1-$^{13}C$]Phe22, [3-$^{13}C$]Ala31-labeled hCT (I) and [1-$^{13}C$]Gly10, [3-$^{13}C$]Ala26-labeled hCT (II), in the monomer and fibril states, respectively, at pH 3.3 and 7.5. The DD-MAS spectrum of I at pH 3.3 (80 mg/mL) exhibits the two signals at 171.4 and 17.2 ppm for the carbonyl carbon of Phe22 and the methyl carbon of the Ala31 residue, respectively (Fig. 2A). Both of the peaks are ascribed to a local random coil form with reference to the conformation-dependent $^{13}C$ chemical shifts; $\alpha$-helix, random coil, and $\beta$-sheet are 171.6, 170.9, and 168.5 ppm for [1-$^{13}C$]Gly; 175.2, 173.2, and 169.0 ppm for [1-$^{13}C$]Phe; and 14.9, 16.9, and 20.0 ppm for [3-$^{13}C$]Ala (Saitô, 1986; Saitô & Ando, 1989; Wishart et al., 1991; Wishart & Sykes, 1994; Saitô et al., 1998). In the case of [1-$^{13}C$]Phe22, we took into account the additional upfield displacement of the peaks by 1.4 ppm, which

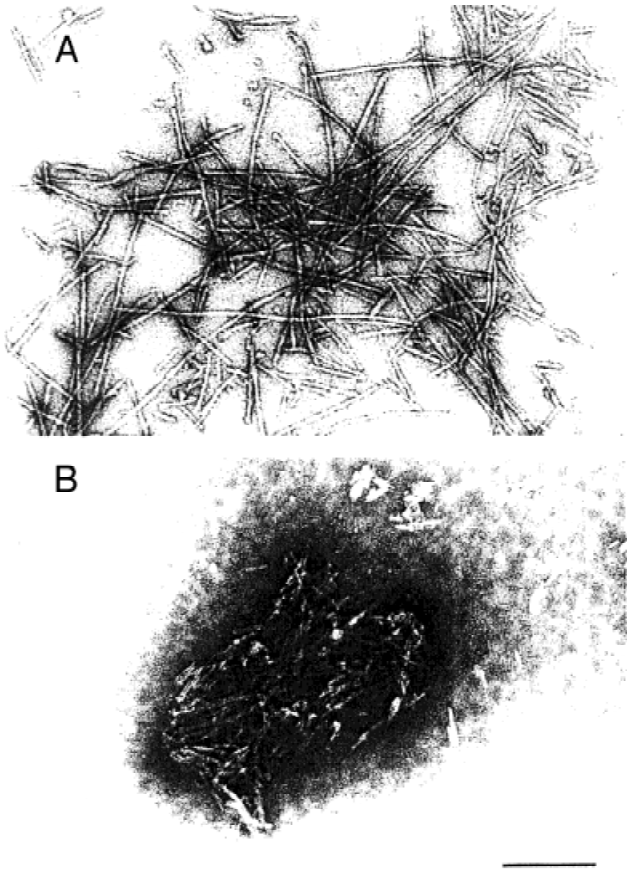


**Fig. 1.** Electron micrographs of hCT fibrils grown (**A**) at pH 3.3 (80 mg/mL) and (**B**) at pH 7.5 (1.5 mg/mL). The samples were negatively stained with 2% (w/v) uranyl acetate. The scale bar represents 200 nm.

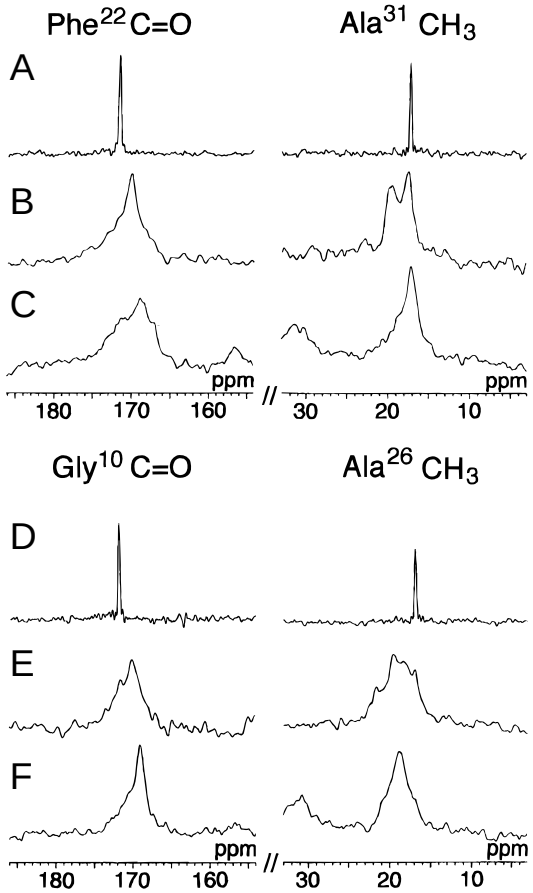


**Fig. 2.** $^{13}$C DD-MAS and CP-MAS NMR spectra of [1-$^{13}$C]Phe22, [3-$^{13}$C]Ala31-labeled hCT (I) (top three traces) and [1-$^{13}$C]Gly10, [3-$^{13}$C]Ala26-labeled hCT (II) (bottom three traces) at pH 3.3 and 7.5. (**A**, **D**) DD-MAS spectra at pH 3.3; (**B**, **E**) CP-MAS spectra of fibril at pH 3.3; (**C**, **F**) CP-MAS spectra of fibril at pH 7.5.

arises for the carbonyl carbon directly bonded to the amide nitrogen of Pro residue (Torchia & Lyerla, 1974; Wishart et al., 1995). Similarly, the $^{13}$C DD-MAS NMR signals of II at 171.8 and 16.9 ppm are assigned to a local $\alpha$-helix form for Gly10 carbonyl and random coil for Ala26 methyl carbons, respectively (Fig. 2D). Accordingly, the hCT monomer in the pH 3.3 solution takes a local $\alpha$-helical conformation around Gly10, and the random coil in the vicinity of Phe22, Ala26, and Ala31.

In the $^{13}$C CP-MAS spectrum (Fig. 2B) of I at pH 3.3 (80 mg/mL), a broad peak at 170.0 ppm and two peaks at 17.2 and 19.7 ppm are observed for Phe22 carbonyl and Ala31 methyl carbons, respectively, and are assigned to the local $\beta$-sheet, and random coil and $\beta$-sheet conformations, respectively. The $^{13}$C CP-MAS NMR signals of Gly10 carbonyl and of Ala26 methyl carbons (II) appear at 169.9 ppm and 16.9, 19.3, and 21.3 ppm, respectively (Fig. 2E), and both residues are assigned to local $\beta$-sheet structures, except for the random coil component from the 16.9 ppm peak of Ala26 methyl carbons. It is noteworthy that conformational changes from the $\alpha$-helix and random coil to the $\beta$-sheet forms occur around the residues of Gly10 (Fig. 2D,E) and Phe22 (Fig. 2A,B), respectively, during the fibril formation. Table 1 summarizes the $^{13}$C chemical shifts of the labeled sites together with their assigned conformations. It is noticeable, however, that the random coil components still remain in the fibril for the Ala26 and Ala31 residues in addition to the converted $\beta$-sheet. Alternatively, it is possible for Ala31 to be assigned to loop-like structure if downfield displacement of peaks (17.2 or 17.3 ppm) from 16.9 ppm are experimentally significant (error range is less than 0.3–0.4 ppm).

Figures 2C and 2F show the $^{13}$C CP-MAS spectra of the hCT fibril (I and II) prepared at pH 7.5. The peak positions of these preparations largely differ from those at pH 3.3, as summarized in Table 1. In particular, the signals of [1-$^{13}$C]Gly10 and [1-$^{13}$C]Phe22 at pH 7.5 are displaced upfield by 0.8 and 1.3 ppm, respectively, compared with those at pH 3.3. The extent of the conformational heterogeneity of the fibril prepared at pH 7.5 is less than those at pH 3.3 as viewed from their line widths, except for Phe22 C=O. These results indicate that the fibril structure is substantially changed by a particular pH condition.

The $^{13}$C NMR spectrum of the reduced form of the $^{13}$C-labeled hCT samples (hCT-SH), which lacks the S–S bridge at the N-terminus, was recorded in a similar manner at pH 3.3 to that of hCT mentioned above (spectra not shown). The DD-MAS signals showed the same chemical shifts as those of the hCT samples (Table 1). In contrast to hCT, turbidity does not develop even after two months. Despite the similar experimental conditions, a large number of transients were needed to obtain the signals with a reasonable S/N ratio in the $^{13}$C CP-MAS spectra comparable to those of hCT. On the contrary, the intensities of $^{13}$C DD-MAS

**Table 1.** *$^{13}C$ chemical shifts of hCT (ppm from TMS) and their assignments*

| | pH 3.3 | | pH 7.5 | pH 3 (hCT-SH) | |
|---|---|---|---|---|---|
| | Monomer[a] | Fibril[b] | Fibril[b] | Monomer[a] | Fibril[b] |
| Gly10 C=O | 171.8 $\alpha$-helix | 169.9 $\beta$-sheet | 169.1 $\beta$-sheet | 171.8 $\alpha$-helix | 169.8 $\beta$-sheet |
| Phe22 C=O | 171.4 random coil | 170.1 $\beta$-sheet | 168.8 $\beta$-sheet | 171.4 random coil | 170.8 random coil |
| | | | 171.5[c] random coil | | 173.0[c] $\alpha$-helix |
| Ala26 $CH_3$ | 6.9 random coil | 16.9 random coil | 18.7 $\beta$-sheet | 16.9 random coil | 16.9 random coil |
| | | 19.3 $\beta$-sheet | | | 20.9 $\beta$-sheet |
| | | 21.3 $\beta$-sheet | | | |
| Ala31 $CH_3$ | 17.2 random coil[d] | 17.3 random coil[d] | 17.0 random coil | 17.2 random coil[d] | 17.3 random coil[d] |
| | | 19.7 $\beta$-sheet | 18.8[c] $\beta$-sheet | | |

[a]Observed in DD-MAS spectra.
[b]Observed in CP-MAS spectra.
[c]Minor peak.
[d]Or loop-like structure (see text).

spectra in hCT-SH were not significantly decreased even after two months. It was noticed that the chemical shifts of Phe22 C=O and Ala26 $CH_3$ of the hCT-SH fibril in the CP-MAS spectra were slightly different from those of the hCT fibril.

*Time-course experiments for hCT fibril formation*

To determine the kinetic property of the conformational transition in the hCT fibrillation process, time courses of the variation of the signal intensities were observed. Variation of the signal intensities for monomer and fibril states can be observed separately in the same sample because the DD-MAS and CP-MAS NMR signals correspond to the monomer and fibril states of hCT, respectively. Acquisition of the $^{13}C$ DD- and CP-MAS spectra was started at 20 °C after 6 h from the dissolution of I (80 mg/mL) in 0.015 M acetic acid solution (pH 3.3) because this time delay was necessary to complete the tight sealing of the sample rotor by glue. It is noteworthy that the signal intensities of the $^{13}C$ DD-MAS spectra decrease gradually with the elapsed time (Fig. 3; left), while those of the $^{13}C$ CP-MAS spectra increase after the delay time as the solution turns viscous to form the gel (Fig. 3; right). On the other hand, the line positions and shapes of the $^{13}C$ DD- and CP-MAS NMR signals for [1-$^{13}C$]Phe22 and [3-$^{13}C$]Ala31 residues did not vary throughout the fibrillation process (Fig. 3). This result indicates that the conformation of hCT monomer and fibril themselves are not changed during the fibril formation. Plots of the resonance intensities for I against the elapsed time (Fig. 4) show that the carbonyl and methyl signals in the DD-MAS spectra decrease gradually until 47 h after dissolution of hCT, and afterward they retain the same intensities. In contrast, those in the CP-MAS spectra for I increase during 9.5–45.5 h. It is also noticed that the extent of the decrease of the Ala31 methyl signal in the DD-MAS spectra (Fig. 4B) is smaller than that of the Phe22 carbonyl signal (Fig. 4A), because the isotropic motion of the methyl group enables one to observe the signal from the fibril component in the DD-MAS spectra. Plots of the signal intensities of the DD- and CP-MAS spectra for [1-$^{13}C$]Gly10 and [3-$^{13}C$]Ala26 (II) against the elapsed time are illustrated in Figure 5. It turns out that the signal intensities of II from the CP-MAS experiments increase after a delay time of 60 h in contrast to the case of I, where the intensities increase after a short delay time of 9 h. The signal intensities of II, obtained from the DD-MAS experiments, decrease after a longer delay time than in the case of I. The reaction rates were analyzed using a two-step autocatalytic reaction model as shown in Figure 6. Details of the kinetic analysis is discussed in the later section.

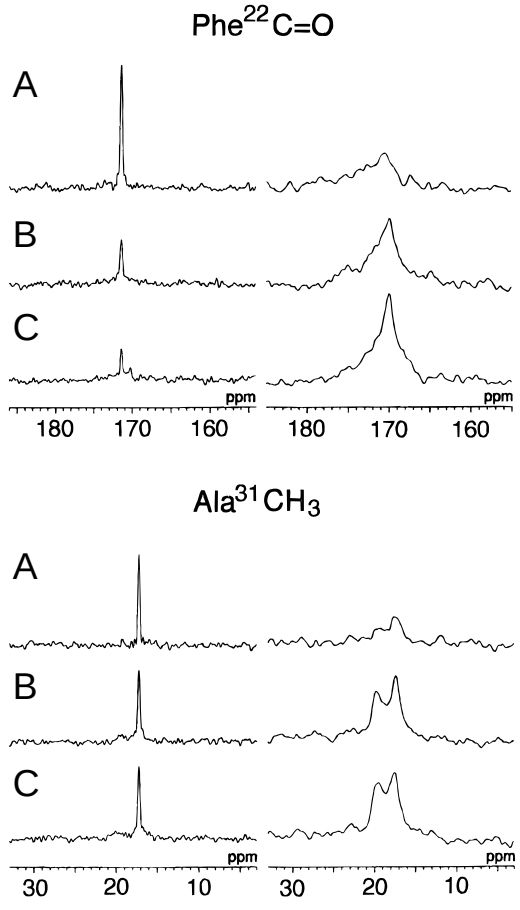


**Fig. 3.** Time course of $^{13}C$ DD-MAS (left panel) and CP-MAS NMR spectra (right panel) of [1-$^{13}C$]Phe22, [3-$^{13}C$]Ala31-labeled hCT (I) dissolved in 0.015 M acetic acid solution at the concentration of 80 mg/mL. pH of the solution was 3.3. Acquisition was started after 6 h from dissolution by accumulating 1,000 scans for DD-MAS and 2,000 scans for CP-MAS experiments: (**A**) 12 h, (**B**) 26.4 h, and (**C**) 179.2 h after dissolution.

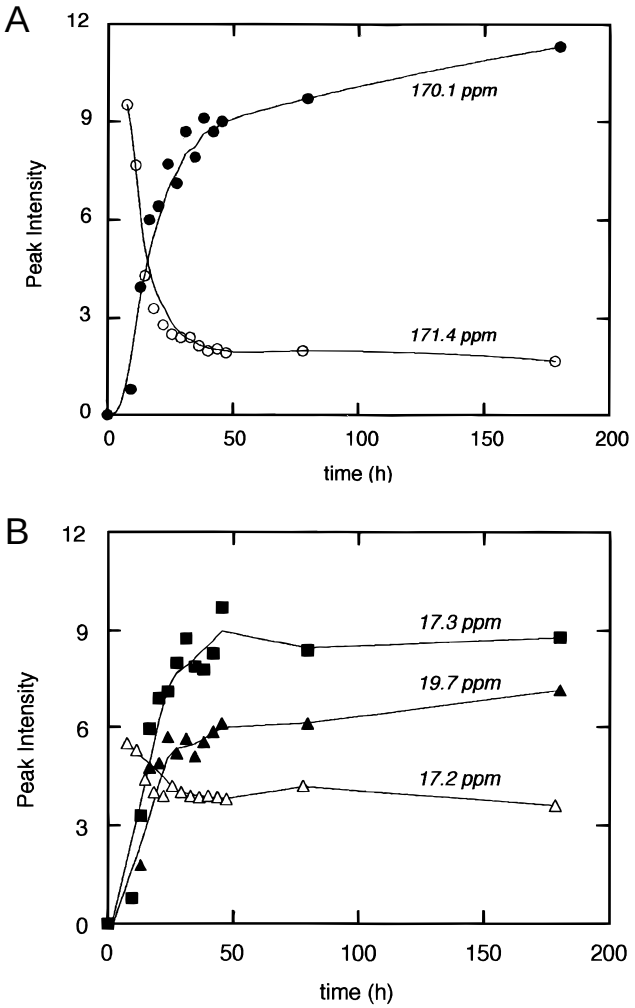


**Fig. 4.** Plots of (**A**) [1-$^{13}$C]Phe22 and (**B**) [3-$^{13}$C]Ala31 peak heights in $^{13}$C DD-MAS and CP-MAS NMR spectra of hCT (I) at pH 3.3 (80 mg/mL) against the elapsed time. The condition is the same as described in Figure 3. The time of dissolution was regarded as 0 h. Open circle, DD-MAS signals; closed circle, CP-MAS signals.

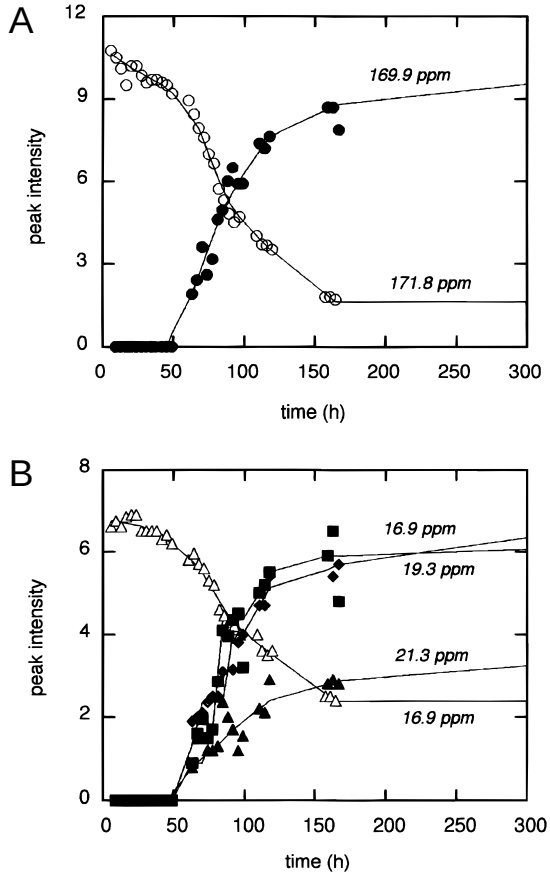


**Fig. 5.** Plots of [1-$^{13}$C]Gly10 and [3-$^{13}$C]Ala31 peak heights in $^{13}$C DD-MAS and CP-MAS NMR spectra of hCT (II) at pH 3.3 (80 mg/mL) against the elapsed time. Sample preparation and plot styles are the same as described in Figures 4 and 5.

Time course of the fibril formation at pH 7.5 was also examined by CD measurements using hCT from natural abundance provided by Ciba-Geigy, because the fibrillation rate at pH 7.5 is too fast to be determined by $^{13}$C NMR measurements (Fig. 6C,D). Monomeric component assigned to random coil (205 nm) decreased gradually as a result of fibril formation after ~3 h since dissolution at the concentration of 0.2 mg/mL. On the other hand, at the higher concentration condition, 1.5 mg/mL, the ellipticity at 205 nm decreased rapidly between 2 and 3 h since dissolution.

## Discussion

### *Conformational transitions of hCT in the process of fibril formation*

It has been demonstrated that the local conformational characterization of peptides and proteins is feasible in view of the conformation-dependent $^{13}$C chemical shifts (Saitô, 1986; Saitô & Ando, 1989; Saitô et al., 1998). Figure 7 illustrates the bar graph presentation of the observed chemical shifts of the $^{13}$C-labeled positions (Fig. 2) vs. a variety of sample preparations (monomer at pH 3.3, sample 1; fibril at pH 3.3, sample 2; fibril at pH 7.5, sample 3) together with those for the reference data of the $\alpha$-helix, $\beta$-sheet, loop-like, and random coil forms for respective residues. Error ranges are also shown at the top of the bars. $^{13}$C chemical shifts referred to TMS shown in the left ordinate and differential shifts with respect to those of random coil (Wishart et al., 1991; Wishart & Sykes, 1994; Saitô et al., 1998) in the right ordinate, respectively. It is therefore evident that the hCT monomer in the acetic acid solution (sample 1) forms a local $\alpha$-helical form around Gly10, although the $\alpha$-helical form has not been well characterized by previous $^1$H NMR studies in aqueous solution (Wüthrich, 1976; Kern et al., 1993). Nevertheless, recent $^1$H NOESY spectra in acetic acid solution showed the evidence for the presence of the $\alpha$-helical conformation in the central region of hCT, but the central helix is shorter than that in 40% TFE/60% $H_2O$ solution (Jeon et al., 1998). In contrast, Phe22 of hCT (sample 1) in the vicinity of Pro23, and Ala26 are found to be involved in a random coil. On the other hand, Ala31 of hCT (sample 1) is suggested to be involved in a loop-like structure in view of the [3-$^{13}$C]Ala31 signal at 17.2 ppm, which is significantly displaced downfield from the peak of the random coil form, 16.9 ppm, with reference to the

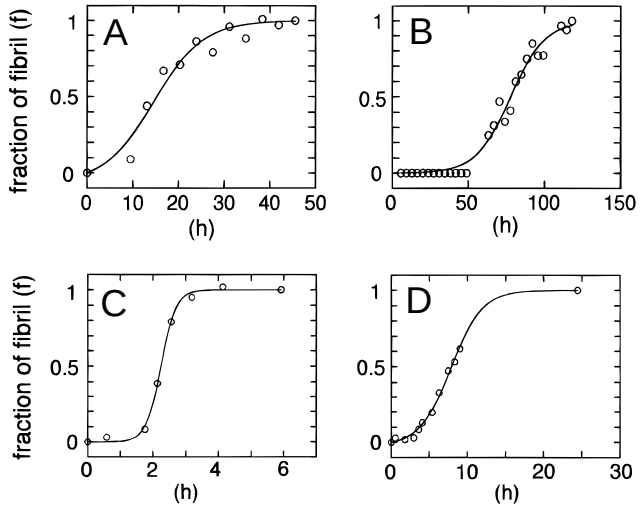


**Fig. 6.** Plots of (**A**) [1-$^{13}$C]Phe22 (I) and (**B**) [1-$^{13}$C]Gly10 (II), peaks in the $^{13}$C CP-MAS NMR spectra in pH 3.3 solution (80 mg/mL) at 20 °C, and plots of the ellipiticity (205 nm) in the CD spectra at pH 7.5 with the concentration of (**C**) 1.5 mg/mL and (**D**) 0.2 mg/mL. Solid lines are the best fits to Equation 7. The vertical line is the fraction of fibril in the system after normalizing the intensities observed at 45.5 and 118 h for **A** and **B**, respectively, using the intensity after dissolution as unity. As for **C** and **D**, the maximum ellipiticity recorded at 0.05 h, because dissolution was taken as 0 and the minimum one recorded at 5.9 (**C**) and 24.4 h (**D**), were taken as 1, respectively.

[3-$^{13}$C]Ala residues in loops of bacteriorhodopsin (17.2–17.8 ppm) (Tanio et al., 1999; Tuzi et al., 1999). The difference of chemical shifts between 16.9 and 17.2 ppm from DD-MAS spectra (Fig. 2A,D) is distinct in view of their narrow signals, as observed for fully hydrated [3-$^{13}$C]Ala-bacteriorhodopsin (Tanio et al., 1999; Tuzi et al., 1999). Interestingly, the local conformation around Gly10 and Phe22 is entirely changed closer to the $\beta$-sheet form during the fibril formation (sample 2), while parts of the Ala26 and Ala31 signals are displaced from the peak positions of the random coil (or loop-like structure) to the typical those of $\beta$-sheet by going from the sample 1 to 2. This means that at least two different conformations are present in the C-terminus region of hCT in the fibril at pH 3.3 (sample 2). It is emphasized that the above-mentioned conformational transition from the $\alpha$-helix to $\beta$-sheet in the central part of hCT is directly observed in this study. Such a conformational change from the $\alpha$-helix to $\beta$-sheet has been reported for polylysine (Greenfield & Fasman, 1969), silk fibroin from *Philosamia cynthia ricini* (Ishida et al., 1990) and amyloid $\beta$-peptide fragments (e.g., Zagorski & Barrow, 1992) in which the conformational transitions are induced depending upon pH or other physical treatments.

Obviously, the conformation of the hCT fibrils at pH 7.5 (sample 3) is different from that at pH 3.3 (sample 2) as viewed from the differential chemical shifts and line shapes in the $^{13}$C CP-MAS spectra. The carbonyl chemical shifts for Gly10 and Phe22 of the latter are closer to those of model peptides forming a typical antiparallel $\beta$-sheet structure (Saitô, 1986; Saitô & Ando, 1989; Saitô

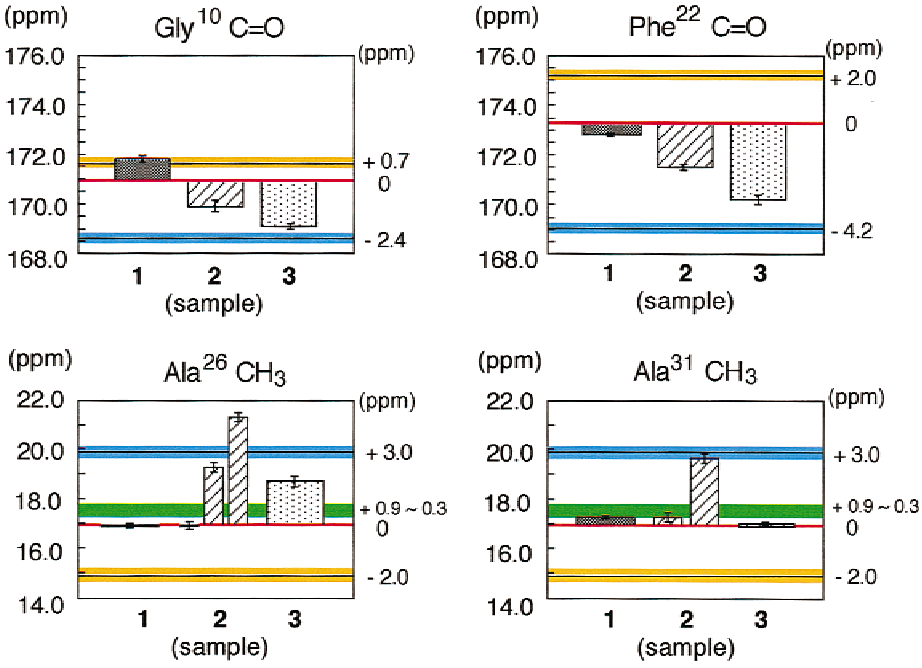


**Fig. 7.** Bar graph presentation of the $^{13}$C chemical shift deviations from those of random coil [the right ordinate (Wishart et al., 1991; Wishart & Sykes, 1994; Saitô et al., 1998)] for each residues vs. a variety of hCT preparations. The left ordinate of the graph shows the $^{13}$C chemical shifts referred to TMS. Cyan band represents the chemical shifts for the typical antiparallel $\beta$-sheet, red; random coil, orange; $\alpha$-helix, green; loop-like structure. Sample 1, monomer in the solution at pH 3.3; sample 2, fibril formed at pH 3.3; and sample 3, fibril formed at pH 7.5. The corrected chemical shifts for Phe22 by 1.4 ppm due to Pro effect (Wishart et al., 1995) are plotted.

et al., 1998) than those of the former. Although there are many possibilities for forming these structures, we suggest here that the mixtures of parallel and antiparallel $\beta$-sheet structures are formed at pH 3.3, and the antiparallel $\beta$-sheet structure alone is produced at pH 7.5, as shown in Figure 8D.

In the suggested model, it is expected that slight deviations of the carbonyl chemical shift values from the antiparallel $\beta$-sheet form for the fibril at pH 3.3 (sample 2) can be ascribed to the formation of a parallel $\beta$-sheet form and/or to a plausible conformational fluctuation for Phe22 in view of its position at the interface between the $\beta$-sheet and random coil forms. The broad resonances observed for the fibril at pH 3.3 (Fig. 2B,E) also support the model because the mixture of parallel and antiparallel $\beta$-sheets causes the conformational heterogeneity. On the other hand, the signal at 21.3 ppm for [3-$^{13}$C]Ala26 in the fibril at pH 3.3 (sample 2) deviates from that of the typical antiparallel $\beta$-sheet. It is probable that this sort of deviation might be again ascribed to the presence of the parallel $\beta$-sheet as proposed by FTIR measurements (Bauer et al., 1994), although no reference $^{13}$C peak for this structure is currently available. Moreover, the two $^{13}$C NMR signals from [3-$^{13}$C]Ala31 at pH 3.3 are evidently ascribed to the two main different conformations, namely random coil and $\beta$-sheet forms, which reflect the presence of the hCT fibrils of antiparallel and parallel $\beta$-sheet domains, respectively, in view of the model in Figure 8D. Further study to clarify this problem is under way in our laboratory based on REDOR experiments (Gullion & Schaefer, 1989; Naito et al., 1996; Nishimura et al., 1998) and synthesis of model peptides to parallel $\beta$-sheet conformation. On the other hand, a single $^{13}$C NMR signal from [3-$^{13}$C]Ala31 appeared at pH 7.5 and assigned to the random coil, because only the antiparallel $\beta$-sheet is formed at this pH, as shown in Figure 8D. It is also possible to explain that the pronounced difference of the chemical shifts of [3-$^{13}$C]Ala26 (18.7 ppm) at pH 7.5 from those of the antiparallel $\beta$-sheet form is attributed to the fact that Ala26 is located in the interface between the antiparallel $\beta$-sheet and random coil regions. Although the $\alpha$-helical components have been observed in the CD spectra (Arvinte et al., 1993) and FTIR spectra (Bauer et al., 1994) of the mature hCT fibrils, we were not able to observe the $\alpha$-helical structure at the $^{13}$C-labeled positions in the fibril sample. However, the existence of the $\alpha$-helical structure in fibril other than the labeled positions is possible, because the $\alpha$-helical component was actually observed in the $^{13}$C CP-MAS spectra of the natural abundance sample (M. Kamihira, A. Naito, S. Tuzi, A.Y. Nosaka, & H. Saito, unpubl. data).

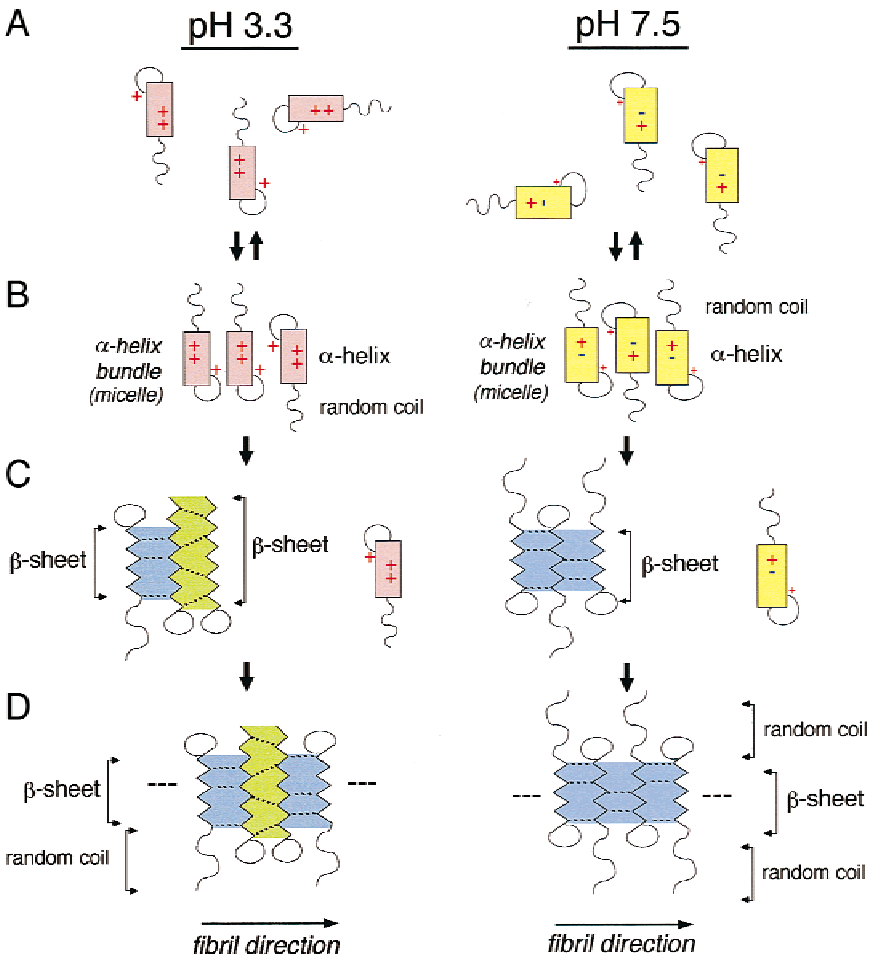


**Fig. 8.** Schematic representation of proposed models for the fibril formation in the cases of pH 3.3 and 7.5. (**A**) hCT monomers in solution; (**B**) a homogeneous association to form the $\alpha$-helical bundle (micelle); (**C**) a homogeneous nucleation process to form the $\beta$-sheet and heterogeneous associating process; (**D**) a heterogeneous fibrillation process to grow a large fibril.

*Kinetics of hCT fibrillation*

The changes of the peak intensities observed in the DD- and CP-MAS spectra (Figs. 3–5) show a two-step reaction process: the first step occurs at ~9.5 h for I, and at ~60 h for II, and the second step appears during 9.5–45.5 h for the former and 60–118 h for the latter. We thus modify the double nucleation mechanism (Ferrone et al., 1980, 1985; Arvinte et al., 1993; Lomakin et al., 1997) to explain this kinetic behavior in this $^{13}C$ NMR study in the following notice: the decrease and increase of the signal intensities obtained from the DD- and CP-MAS spectra, respectively, are synchronously changed. This fact indicates that there exists the conformational transition from monomer to fibril state. Another important observation is a certain delay time followed by the decrease and increase of the signal intensities of DD- and CP-MAS spectra, respectively. This kinetic property can be explained by considering an autocatalytic reaction from one species (A) to the other (B). If we adopt a two-step autocatalytic reaction mechanism for the fibril formation, the first reaction step is a homogeneous nucleation process and the second step implies a heterogeneous fibrillation process. A is the component of hCT molecule (A form) observable by the DD-MAS experiments, and B is that (B form) observable by the CP-MAS experiments. To analyze the experimentally obtained kinetic properties, we assume that micelles with the same aggregation number $n_0$ are formed as a solubilized primary process in the solution (Lomakin et al., 1997) (Fig. 8A,B),

$$n_0 A \text{ (monomers)} \rightleftarrows A_{n_0} \text{ (micelle)}. \quad (1)$$

Naturally, we assume that hCT molecules in the monomer and micelle states show the same DD-MAS NMR signals. The micelle corresponds to the $\alpha$-helix bundle, as previously suggested (Kanaori & Nosaka, 1995). We consider the case where the total hCT concentration of A form ($[A_T]$), which gives rise to DD-MAS signals, is always much higher than the critical micellar concentration $c^*$. Under these conditions, the first reaction step can be given by

$$A_{n_0} \xrightarrow{k_1} B_{n_0}, \quad (2)$$

where $A_{n_0}$ is the micelles with $n_0$ number of hCT monomers (A form) and $B_{n_0}$ is the nucleus of fibril consisting of $n_0$ number of hCT molecules (B form) (Fig. 8B,C). The signal of $B_{n_0}$ can be observed by CP-MAS experiments. Because $[A_T] = n_0[A_{n_0}] + c^*$ is much higher than $c^*$, $[A_{n_0}]$ can be expressed as $[A_T]/n_0$. When the initial concentration of hCT in the solution is denoted as $a, k_1$ is the rate constant, and $f$ is the fraction of B form in the system, the kinetic equation for the Reaction 2 can be given by

$$(df/dt)_1 = k_1(1 - f). \quad (3)$$

The second heterogeneous fibrillation process can be expressed as

$$A + B_n \xrightarrow{k_2} B_{n+1}, \quad (4)$$

where $k_2$ is the rate constant of the Reaction 4 and $B_n$ and $B_{n+1}$ are the elongated fibrils with $n$ and $n + 1$ numbers of hCT molecules (B form) (Fig. 8C,D), respectively. In this process, we assume that each hCT molecules in $B_n$ can act as catalytic sites to accelerate the change from A form to B form. Thus, $[B_n]$ can be replaced by $[B] = n_0[B_{n_0}] + (n_0 + 1)[B_{n_{0+1}}] + \cdots + n[B_n] + \cdots = af$ in the kinetic Equation 4. Although micelles are formed, we consider that individual hCT molecules (A form) react with $B_n$. As a consequence of the Reaction 4, $[A_T] = a(1 - f)$ can be used as [A], and [B] increases stepwise after a certain delay time. The relevant differential equation is given by

$$(df/dt)_2 = k_2 af(1 - f). \quad (5)$$

The overall kinetic equation can be expressed as

$$(df/dt) = (df/dt)_1 + (df/dt)_2 = k_1(1 - f) + k_2 af(1 - f). \quad (6)$$

This differential equation can be integrated to give

$$f = \frac{\rho\{\exp[(1 + \rho)kt] - 1\}}{\{1 + \rho \exp[(1 + \rho)kt]\}}, \quad (7)$$

under the boundary condition of $t = 0$ and $f = 0$, where $k = k_2 a$, and $\rho$ represents the dimensionless value to describe the ratio of $k_1$ to $k$. Using Equation 7, we have analyzed the process of fibril formation at pH 3.3 and 7.5. The best fits for the plots of signal intensities obtained from the CP-MAS and CD experiments, against the elapsed time, are shown in Figure 6, and the kinetic parameters are summarized in Table 2. Here, $a$ = 23.4 mM (80 mg/mL) and 0.439 mM (1.5 mg/mL) or 58.5 $\mu$M (0.2 mg/mL) are used for CP-MAS and CD experiments, respectively. Because the carbonyl signals do not show splitting and the separation between the components obtained by the DD- and CP-MAS experiments is better than in the case of the methyl signal, we use the carbonyl signal for the kinetic analysis. The most striking feature in the kinetic analysis at pH 3.3 is that the $k_1$ values are three to five and one to three orders of magnitude smaller than the $k_2$ and $ak_2$ (effective rate constant of Reaction 4) values, respectively. These results suggest that the first homogeneous nucleation process is much slower than the second heterogeneous fibrillation process. It is also noted that the $k_2$ values are similar for the samples shown in Figures 4 and 5, whereas the $k_1$ values are quite different for the two samples, reflecting the large difference of the delay time of the stepwise increase of the signal intensities. The large difference in $k_1$ values suggests that the homogeneous nucleation is strongly sensitive to salt concentration or to only a little impurity, etc., and hence, the rate for II is actually slower in this process than for I (Figs. 4, 5). The second step must be a heterogeneous maturing and associating process between the hCT monomers and the nuclei; thus, we call the second step a heterogeneous fibrillation process. This process causes an increase of the peak intensities observed in the CP-MAS spectra. A fibrillation process derived by the kinetic analysis is illustrated in Figure 8. It is evident that there are at least two time determining processes to show a stepwise manner of autocatalytic reaction and expressed by Reactions 2 (Fig. 8B,C) and 4 (Fig. 8C,D). Although many other fast reactions may exist during the process of large fibril formation, the secondary structure and the chemical environments of the components observed in the DD- and CP-MAS spectra did not change throughout this process, and no additional peaks were observed (Fig. 3). These findings in $^{13}C$ NMR experiments imply that it is enough to consider the two-step reactions for the fibrillation kinetics. Therefore, it is also mentioned that the present NMR approach can be straightforwardly extended to clarify fibrillation kinetics of Alzheimer $\beta$ peptides (Jarrett et al.,

**Table 2.** *Rate constants,* $k_1$ *and* $k_2$*, for hCT fibril formation of various preparations*

| Method | Sample | Concentration pH | $k_1$ ($s^{-1}$) | $k_2$ ($s^{-1}M^{-1}$) | $ak_2$ ($s^{-1}$)[c] |
|---|---|---|---|---|---|
| NMR[a] | I | 80 mg/mL pH 3.3 | $3.28(\pm0.56) \times 10^{-6}$ | $2.04(\pm0.49) \times 10^{-3}$ | $4.10(\pm1.15) \times 10^{-5}$ |
| NMR[a] | II | 80 mg/mL pH 3.3 | $2.71(\pm0.11) \times 10^{-8}$ | $1.04(\pm0.08) \times 10^{-3}$ | $2.11(\pm0.19) \times 10^{-5}$ |
| CD[b] | hCT(Ciba-Geigy) | 1.5 mg/mL pH 7.5 | $6.44(\pm0.29) \times 10^{-8}$ | $2.78(\pm0.19)$ | $1.22(\pm0.08) \times 10^{-3}$ |
| CD[b] | hCT(Ciba-Geigy) | 0.2 mg/mL pH 7.5 | $2.79(\pm0.04) \times 10^{-6}$ | $2.29(\pm0.14)$ | $1.34(\pm0.08) \times 10^{-4}$ |

[a]Based on the carbonyl signals in the $^{13}C$ CP-MAS NMR spectra at 20 °C.
[b]Based on an absorbance at 205 nm of CD spectra at 25 °C.
[c]$a$ is the initial concentration of hCT and 23.4, 0.439, and 58.5 mM are used for the concentration of 80, 1.5, and 0.2 mg/mL, respectively.

1993; Lomakin et al., 1996), or other amyloid peptides in relation to their pathogenesis.

The same analysis is applied to the case of hCT fibril formation at pH 7.5 (Fig. 6C,D). The kinetic parameters are summarized in Table 2. It is clear that the fibril formation after the nucleation at pH 7.5 occurred much faster than that at pH 3.3 because $k_2$ values at pH 7.5 were three orders of magnitude larger than that at pH 3.3, while $k_1$ values were not different among them. We noticed that $k_2$ values are not varied with the change of concentration (rows 3 and 4 in Table 2). We also realized that $k_1$ values are not correlated with pH and concentration from the present observation.

### *Molecular mechanism of the fibril formation*

It was shown that the second step of fibril formation at pH 7.5 is much faster than that at pH 3.3 (Arvinte & Ryman, 1992), and the conformation of the fibril at pH 7.5 is different from that at pH 3.3. This difference is caused by the changes in molecular interactions among the charged side chains such as Asp15, Lys18, and His20. At pH 3.3, the side chains of Lys18 and His20 as well as the amino group of Cys1 are expected to be positively charged and located at nearly opposite sides in the amphiphilic $\alpha$-helical wheel of the hCT molecule (Epand et al., 1983), whereas Asp15 is neutral. It was suggested that hCT monomers aggregate to form an $\alpha$-helical bundle by a hydrophobic interaction in the first nucleation process (Kanaori & Nosaka, 1995). We therefore propose a molecular mechanism of fibril formation as depicted in Figure 8 as one of the possible models. The interaction to assemble can be attenuated by the unfavorable electrostatic interactions between the positively charged side chains of Lys18 and His20, and the amino group of Cys1 at pH 3.3. On the other hand, at pH 7.5 the side chain of Lys18 is protonated with a positive charge, and that of Asp15 is deprotonated with a negative charge, leading to the fast fibrillation. The electrostatic interaction of the positively and negatively charged side chains between the hCT molecules may assemble the hCT in an antiparallel way at pH 7.5, where the positively charged side chains associate in both parallel and antiparallel ways at pH 3.3 (Fig. 8B). Subsequently, these $\alpha$-helical bundles (micelle) change the conformation to an oligomeric $\beta$-sheet as the first nucleation step (Fig. 8C). Maturation process (Fig. 8C,D) results in formation of long fibrils parallel to the arrows, as indicated in Figure 8D. As illustrated in Figure 8C, a homogeneous fibril with an antiparallel $\beta$-sheet conformation in the central region and a random coil in the C-terminus region is formed at pH 7.5, whereas the heterogeneous fibril, with a mixture of parallel $\beta$-sheets in the entire region and antiparallel $\beta$-sheets in the central region, are formed at pH 3.3. The amino group of Cys1 also protonates partially at pH 7.5. This might cause the electrostatic interaction between the ionized amino group and the side chain of Asp15, which would induce the heterogeneity of fibril structure if any. Using this model, an $\alpha$-helical bundle (micelle) has to simultaneously change its conformation from an $\alpha$-helix to a $\beta$-sheet in the first nucleation process, while one $\alpha$-helix can be converted to a $\beta$-sheet in the second heterogeneous fibrillation process. This interpretation explains why the second process is much faster than the first. Such an $\alpha$-helical macrodipole has been proposed for the formation of amyloid deposits in Alzheimer's disease through a conversion from an $\alpha$-helix to a $\beta$-sheet (Zagorski & Barrow, 1992).

It has been reported that hCT analogues, without a S–S bridge between Cys1 and Cys7, have only a weak activity (Orlowski et al., 1987). We found that the hCT-SH molecule lacking the disulfide bridge does not show turbidity. However, the observation of weak resonances in the CP-MAS spectra was ascribed to the presence of fibrils. Thus, the conformation of the hCT-SH fibril seems to be slightly different from that of the hCT fibril, as manifested from the chemical shifts observed in the CP-MAS spectra. This result suggests that the S–S bridge plays an essential role for maturing of the hCT fibril. It has been reported for sCT that the S–S loop promotes the formation of a helical structure (Goltzman, 1980). Further, the formation of helical-like structure in the loop was reported for sCT (Motta et al., 1991a). It is therefore expected for the hCT that the N-terminus S–S loop is required to stabilize the amphiphilic $\alpha$-helices in the N-terminus to the central region because the primary structure at the N-terminal 1–10 segment is highly conserved between sCT and hCT (Keutmann et al., 1970). It is important to point out that the inhibition of the $\alpha$-helical formation in the N-terminus for hCT–SH will reduce the association with monomers in the first nucleation process as well as in the second fibrillation process.

## Conclusions

It is demonstrated by directly observing the conformational change at specific sites using $^{13}$C-labeled hCT molecules by solid-state NMR spectroscopy that there occurs a local conformational transition from an $\alpha$-helix to a $\beta$-sheet in the central region of hCT in the process of fibril formation. The pH difference between 3.3 and 7.5 causes the structural changes of the fibrils: not only the hydrophobic interaction but also the electrostatic interaction acts to form the fibril at pH 7.5, whereas only the hydrophobic interaction plays an essential role at pH 3.3. From the kinetic analysis, it appears that the fibril formation occurs in the following steps: the first step is a homogeneous process, which associates the $\alpha$-helix of a hCT monomer with that of other monomer to form $\beta$-sheet structures. The second step is an autocatalytic heterogeneous process, which associates the existing fibril with a hCT monomer to produce larger fibrils. It also appears that the first step does not depend on the pH values, but the second step does. The reaction rate for the first step is much slower than that for the second step, because in the first step two $\alpha$-helices are simultaneously converted to $\beta$-sheets in contrast to the second step where only one $\alpha$-helix is converted to a $\beta$-sheet. It is also shown that the S–S bridge in the N-terminus of hCT plays a crucial role for fibril formation because the $\alpha$-helix in the N-terminus is stabilized by the S–S bridge.

## Materials and methods

### *Materials*

Unlabeled hCT was provided by Ciba-Geigy Pharmaceuticals (Basel, Switzerland). Two types of $^{13}$C-labeled hCT were synthesized by means of Fmoc chemistry using an Applied Biosystems 431A peptide synthesizer: [1-$^{13}$C]Phe22, [3-$^{13}$C]Ala31-labeled hCT (I) and [1-$^{13}$C]Gly10, [3-$^{13}$C]Ala26-labeled hCT (II). Fmoc-amino acids were purchased from Peptide Institute (Osaka, Japan). Fmoc $^{13}$C-labeled amino acids (99% enriched) were synthesized by the reaction of Fmoc-Osu with the 1-$^{13}$C or 3-$^{13}$C–labeled amino acids (from CIL, Andover, Massachusetts) following the method of Paquet (1982). We used an amide resin (Applied Biosystems, Inc., Foster City, California) for the C-terminus proline amidation. The peptides were purified by reversed-phase high-performance liquid chromatography (HPLC) using a mixture of water and acetonitrile containing 0.05% TFA as a mobile phase, after deprotection and cleavage from the resin. The disulfide bridge between Cys1 and Cys7 was formed overnight by air oxidation at pH 8.0–8.5 with diluted concentration in the presence of 6 M urea to prevent fibrillation (Kanaori & Nosaka, 1996). The reaction was stopped by adding acetic acid solution and then the crude hCT preparation was purified by HPLC. The disulfide bond formation was confirmed by the absence of free SH groups by the method of Ellman (1959). The hCT was lyophilized directly from aqueous solution after the HPLC purification and used for fibril formation as described below.

For the structure determination, hCT was dissolved in 0.015 M acetic acid solution (80 mg/mL) at pH 3.3, and the fibril in a turbid gel was formed after a certain delay time. The fibril samples, without forming a gel, were prepared by dissolving a low concentration of hCT powder (1.5 mg/mL) in 0.1 M sodium acetate solution at pH 7.5 and stirring overnight. After removing the supernatant, fibril component was packed in the NMR rotor.

For the time course of the NMR experiments, the lyophilized preparations thus obtained were dissolved in 0.015 M acetic acid solution at pH 3.3, because the fibrillation in the acidic condition proceeds more slowly when compared with that in the neutral condition (Arvinte & Ryman, 1992). It is therefore possible to reveal any conformational change accompanied by the fibrillation, through NMR measurements. Immediately after hCT (80 mg/mL) was dissolved in the acidic solution, a portion of the solution (80 $\mu$L) was placed in a 5-mm-o.d. zirconia rotor for the $^{13}$C NMR studies and sealed with Araldite® (Ciba-Geigy) to prevent evaporation of the mother liquor throughout the NMR measurements. The same solution was separately transferred to a test tube at the same temperature as used in the NMR measurements to check the turbidity of the solution by visual observation.

### *Methods*

#### *NMR measurements*

All $^{13}$C NMR spectra were recorded on a Chemagnetics CMX 400 NMR spectrometer at the resonance frequency of 100.6 MHz. The $^{13}$C NMR spectra were obtained by a CP-MAS combined with a TOSS (total suppression of spinning side bands) pulse sequence (Dixon, 1982) and DD-MAS techniques. It is established that the CP-MAS method (combination of cross-polarization, high-power dipolar decoupling, and magic-angle spinning) can give signals of the solid component, which is fibril in this case. In contrast, the DD-MAS method (combination of 90° pulse excitation, high-power proton dipolar decoupling, and magic-angle spinning) mainly gives signals from the solution component, which is monomeric for the carbonyl carbons and both monomeric and fibril components for the methyl carbons in view of their spin-lattice relaxation times, compared with repetition times. The $^{13}$C chemical shifts were calibrated by using the external carboxyl peak of crystalline glycine at 176.0 ppm from tetramethylsilane (TMS). Accuracy of the chemical shifts in the DD- and CP-MAS experiments were within $\pm$0.1 and 0.3 ppm, respectively. The $\pi/2$ pulse lengths for the carbon and proton nuclei were 4.6–5.3 $\mu$s, and the recycle delay times were 4 and 5 s for the CP-MAS and DD-MAS studies, respectively. All NMR measurements were performed at 20 °C. The number of accumulations for the DD- and CP-MAS signals was 1,000 and 2,000, respectively, in the time-course studies. For the other studies, the transients were accumulated until a reasonable S/N ratio was achieved.

#### *Electron microscope observation*

For electron microscopic analyses, hCT fibrils formed after standing 2 days in 0.015 M acetic acid (80 mg/mL, pH 3.3) and 3 days in 0.1 M sodium acetate solution (1.5 mg/mL, pH 7.5) were diluted with each solution to prepare the fibril dispersed suspension. Five microliters of the suspension was placed on a Formvar-covered grid and stained with 5 $\mu$L of 2% (w/v) uranyl acetate and air dried after removal of excess liquid with filter paper. Measurements of electron microscopy were performed on a JEOL 1200 EX II electron microscope operating at 80 kV.

#### *CD measurement*

CD measurements were performed on an AVIV model 62DS using quartz cuvettes with path lengths of 0.02 and 0.2 cm. Ellipticity at 205 nm in the negative peak was recorded against the elapsed time. The hCT concentrations were 1.5 mg/mL (0.439 mM) or 0.2 mg/mL (58.5 $\mu$M), and 20 mM phosphate buffer (pH 7.5) was used. Temperature was controlled to 25 °C using thermostatted cell holder throughout the CD measurements.

## Acknowledgments

We thank Dr. M. Takai from International Research Laboratories, Ciba-Geigy Japan for technical advice for the synthesis of hCT. We are also indebted to Drs. S. Sonobe, T. Shimmen, S. Kimura, and T. Iyanagi of Himeji Institute of Technology for their help and advice in measuring the electron microscopy and the CD measurements. This work was supported, in part, by Grants-in-Aid for Scientific Research from the Ministry of Education, Science, Culture and Sports of Japan (09558094, 09640612, 0645466, 09261233, and 10179217). One of the authors (M.K.) is grateful to the Research Fellowships for Young Scientists from the Japan Society for the Promotion of Science.

## References

Arvinte T, Cudd A, Drake AF. 1993. The structure and mechanism of formation of human calcitonin fibrils. *J Biol Chem 268*:6415–6422.

Arvinte T, Ryman K. 1992. Pharmaceutical compositions comprising calcitonin. European Patent Application, Publication number 0490549A1.

Austin LA, Heath H. 1981. Calcitonin: Physiology and pathophysiology. *N Engl J Med 304*:269–278.

Bauer HH, Müller M, Goette J, Merkle HP, Fringeli UP. 1994. Interfacial adsorption and aggregation associated changes in secondary structure of human calcitonin monitored by ATR-FTIR spectroscopy. *Biochemistry 33*:12276–12282.

Cohen FE, Pan KM, Huang Z, Baldwin M, Fletterick RJ, Prusiner SB. 1994. Structural clues to prion replication. *Science 264*:530–531.

Copp DH. 1970. Endocrine regulation of calcium metabolism. *Annu Rev Physiol 32*:61–86.

Copp DH, Cameron EC, Cheney BA, Davidson AGF, Henze KG. 1962. Evidence for calcitonin. A new hormone from the parathyroid that lowers blood calcium. *Endocrinology 70*:638–649.

Dixon WT. 1982. Spinning-sideband-free and spinning-sideband-only NMR spectra in spinning samples. *J Chem Phys 77*:1800–1809.

Doi M, Kobayashi Y, Kyogoku Y, Takimoto M, Goda K. 1990. Structure study of human calcitonin. In: River JE, Marshall GR, eds. *Peptides: Chemistry, structure & biology*. La Jolla, California, 11th Proc Am Pept Symp, July 9–14, 1989. pp 165–167.

Ellman GL. 1959. Tissue sulfhydryl groups. *Arch Biochem Biophys 82*:70–77.

Epand RM, Epand RF, Orlowski RC, Schlueter RJ, Boni LT, Hui SW. 1983. Amphipathic helix and its relationship to the interaction of calcitonin with phospholipids. *Biochemistry 22*:5074–5084.

Ferrone FA, Hofrichter J, Eaton WA. 1985. Kinetics of sickle hemoglobin polymerization. II. A double nucleation mechanism. *J Mol Biol 183*:611–631.

Ferrone FA, Hofrichter J, Sunshine HR, Eaton WA. 1980. Kinetic studies on photolysis-induced gelation of sickle cell hemoglobin suggest a new mechanism. *Biophys J 32*:361–380.

Goltzman D. 1980. Examination of interspecies differences in renal and skeletal receptor binding and adenylate cyclase stimulation with human calcitonin. *Endocrinology 106*:510–518.

Greenfield N, Fasman GD. 1969. Computed circular dichroism spectra for the evaluation of protein conformation. *Biochemistry 8*:4108–4116.

Gullion T, Schaefer J. 1989. Rotational-echo double-resonance NMR. *J Magn Reson 81*:196–200.

Habener JF, Singer FR, Deftos LJ, Neer RM, Potts JT Jr. 1971. Explanation for unusual potency of salmon calcitonin. *Nat New Biol 232*:91–92.

Ishida M, Asakura T, Yokoi M, Saitô H. 1990. Solvent- and mechanical-treatment-induced conformational transition of silk fibroins studies by high-resolution solid-state $^{13}$C NMR spectroscopy. *Macromolecules 23*:88–94.

Jarrett JT, Berger EP, Lansbury PT Jr. 1993. The carbonyl terminus of the $\beta$ amyloid protein is critical for the seeding of amyloid formation: Implication for the pathogenesis of Alzheimer's disease. *Biochemistry 32*:4693–4697.

Jeon YH, Kanaori K, Takashima H, Kosiba T, Nosaka YA. 1998. Comparative studies on human calcitonin fibrillation in aqueous and trifluoroethanol solution by proton NMR spectroscopy. *Proc ICMRBS XVIII*. Tokyo. p 61.

Kanaori K, Nosaka AY. 1995. Study of human calcitonin fibrillation by proton nuclear magnetic resonance spectroscopy. *Biochemistry 34*:12138–12143.

Kanaori K, Nosaka AY. 1996. Characterization of human calcitonin fibrillation in aqueous urea solution by $^{1}$H NMR spectroscopy. *Biochemistry 35*:12671–12676.

Kern D, Drakenberg T, Wikström M, Forsén S, Bang H, Fischer G. 1993. The *cis*/*trans* interconversion of the calcium regulating hormone calcitonin is catalyzed by cyclophilin. *FEBS Lett 323*:198–202.

Keutmann HT, Parsons JA, Potts JT Jr, Schlueter RJ. 1970. Isolation and chemical properties of two calcitonins from salmon ultimobranchial glands. *J Biol Chem 245*:1491–1496.

Kumar MA, Foster GV, MacIntyre I. 1963. Further evidence for calcitonin. A rapid-acting hormone which lowers plasma-calcium. *Lancet* 480–482.

Lomakin A, Chung DS, Benedek GB, Kirschner DA, Teplow DB. 1996. On the nucleation and growth of amyloid $\beta$-protein fibrils: Detection of nuclei and quantitation of rate constants. *Proc Natl Acad Sci USA 93*:1125–1129.

Lomakin A, Teplow DB, Kirschner DA, Benedek GB. 1997. Kinetics theory of fibrillogenesis of amyloid $\beta$-protein. *Proc Natl Acad Sci USA 94*:7942–7947.

Meadows RP, Nikonowicz EP, Jones CR, Bastian JW, Gorenstein DG. 1991. Two-dimensional NMR and structure determination of salmon calcitonin in methanol. *Biochemistry 30*:1247–1254.

Meyer JP, Pelton JT, Hoflack J, Saudek V. 1991. Solution structure of salmon calcitonin. *Biopolymers 31*:233–241.

Motta A, Pastore A, Goud NA, Castiglione MM. 1991a. Solution conformation of salmon calcitonin in sodium dodecyl sulfate micelles as determined by two-dimensional NMR and distance geometry calculations. *Biochemistry 30*:10444–10450.

Motta A, Temussi PA, Wünsch E, Bovermann G. 1991b. A $^{1}$H NMR study of human calcitonin in solution. *Biochemistry 30*:2364–2371.

Naito A, Nishimura K, Kimura S, Tuzi S, Aida M, Yasuoka N, Saitô H. 1996. Determination of the three-dimensional structure of a new crystalline form of N-Acetyl-Pro-Gly-Phe as revealed by $^{13}$C REDOR, X-ray diffraction and molecular dynamics calculation. *J Phys Chem 100*:14995–15004.

Nishimura K, Naito A, Tuzi S, Saitô H, Hashimoto C, Aida M. 1998. Determination of the three-dimensional structure of crystalline Leu-enkephaline dihydrate based on six sets of accurately determined interatomic distances from $^{13}$C REDOR NMR and the conformation dependent $^{13}$C chemical shifts. *J Phys Chem 102*:7476–7483.

Orlowski RC, Epand RM, Stafford AR. 1987. Biologically potent analogues of salmon calcitonin which do not contain an N-terminal disulfide-bridged ring structure. *Eur J Biochem 162*:399–402.

Paquet A. 1982. Introduction of 9-fluorenylmethyloxycarbonyl, trichloroethoxycarbonyl, and benzyloxycarbonyl amine protecting groups into *O*-unprotected hydroxyamino acids using succinimidyl carbonates. *Can J Chem 60*:976–980.

Rittel W, Maier R, Brugger M, Kamber B, Riniker B, Sieber P. 1976. Structure–activity relationship of human calcitonin. III. Biological activity of synthetic analogues with shortened or terminally modified peptide chains. *Experientia 32*:246–248.

Saitô H. 1986. Conformation-dependent $^{13}$C chemical shifts: A new means of conformational characterization as obtained by high-resolution solid-state NMR. *Magn Res Chem 24*:835–852.

Saitô H, Ando I. 1989. High-resolution solid-state NMR studies of synthetic and biological macromolecules. *Annu Rep NMR Spectrosc 21*:209–290.

Saitô H, Tuzi S, Naito A. 1998. Empirical versus nonempirical evaluation of secondary structure of fibrous and membrane proteins by solid-state NMR: A practical approach. *Annu Rep NMR Spectrosc 36*:79–121.

Samuel RE, Salmon ED, Briehl RW. 1990. Nucleation and growth of fibres and gel formation in sickle cell haemoglobin. *Nature 345*:833–835.

Sieber P, Riniker B, Brugger M, Kamber B, Rittel W. 1970. Human calcitonin. VI. Synthesis of calcitonin M. *Helv Chim Acta 53*:2135–2150.

Sipe JD. 1992. Amyloidosis. *Annu Rev Biochem 61*:947–975.

Tanio M, Tuzi S, Yamaguchi S, Kawaminami R, Naito A, Needleman R, Lanyi JK, Saitô H. 1999. Conformational changes of bacteriorhodopsin along the proton-conduction chain as studied with $^{13}$C NMR of [3-$^{13}$C]Ala-labeled protein: Arg82 may function as an information mediator. *Biophys J 77*:1577–1584.

Taubes G. 1996. Misfolding the way to disease. *Science 271*:1493–1495.

Torchia DA, Lyerla JR Jr. 1974. Molecular mobility of polypeptides containing proline as determined by $^{13}$C magnetic resonance. *Biopolymers 13*:97–114.

Tuzi S, Yamaguchi S, Tanio M, Konishi H, Inoue S, Naito A, Needleman R, Lanyi JK, Saitô H. 1999. Location of a cation-binding site in the loop between helices F and G of bacteriorhodopsin as studied by $^{13}$C NMR. *Biophys J 76*:1523–1531.

Wishart DS, Bigam CG, Holm A, Hodges RS, Sykes BD. 1995. $^{1}$H, $^{13}$C and $^{15}$N random coil NMR chemical shifts of the common amino acids. I. Investigations of nearest-neighbor effects. *J Biomol NMR 5*:67–81.

Wishart DS, Sykes BD. 1994. Chemical shifts as a tool for structure determination. *Methods Enzymol 239*:363–392.

Wishart DS, Sykes BD, Richards FM. 1991. Relationship between nuclear magnetic resonance chemical shift and protein secondary structure. *J Mol Biol 222*:311–333.

Wüthrich K. 1976. *NMR in biological research: Peptides and proteins*. Amsterdam, Holland: North-Holland Publishing Company. pp 65–72.

Zagorski MG, Barrow CJ. 1992. NMR studies of amyloid beta-peptides: Proton assignments, secondary structure, and mechanism of an alpha-helix $\rightarrow$ beta-sheet conversion for a homologous, 28-residue, N-terminal fragment. *Biochemistry 31*:5621–5631.